Available online at www.sciencedirect.com
SCIENCE DIRECT®
Sensors and Actuators A 105 (2003) 76–82
SENSORS AND ACTUATORS A PHYSICAL
www.elsevier.com/locate/sna

PCB-integrated metallic thermal micro-actuators

Eniko T. Enikov*, Kalin Lazarov

Department of Aerospace and Mechanical Engineering, The University of Arizona, 1130 N. Mountain, Tucson, AZ 85721, USA

Received 7 October 2002; received in revised form 18 February 2003; accepted 19 February 2003

Abstract

The development of thermal micro-actuators on printed circuit boards is described. The fabricated metal actuators are shown to have similar displacement characteristics when compared with silicon-based devices described in the literature. The actuators are benchmarked with respect to power consumption, stroke, and response time. It is further demonstrated that simple analytical estimates for the response time are in good agreement with the experimental measurements and finite element analysis. The thermal cooling transient times are captured using a two-step constant-current excitation method. The fabrication process and potential application areas of the developed device are also provided.

Keywords: Thermal micro-actuator; Micro-relay; Thermal response time; MEMS

1. Introduction and motivation

In comparison with electrostatic and piezo-electric actuators, thermal micro-actuators hold promise for larger displacements and low actuation voltages. In multi-band radio frequency applications, it is often necessary to tune the impedance of the front-end circuits over a large range of values, requiring switching between different banks of impedance matching elements [1]. In such instances, it is desirable to eliminate cross-talk, e.g. to achieve large electrical isolation between the contacts of the RF switch.

Thermal micro-actuators are a promising solution to the need for large-displacement, low-power MEMS actuators. Potential applications of these devices are micro-relays, tunable impedance RF networks, and miniature medical instrumentation. The first thermal actuators developed for such applications were made through thin film deposition of polycrystalline silicon (polysilicon) [2,3]. In the last five years though, the range of materials used for thermal actuators has been expanded to metals [4,5] and single-crystal silicon [6,7]. While polysilicon devices have the advantage of ease of integration with on-chip electronics and relatively low-power consumption (86 mW [8]), the polysilicon layers are only a few microns thick, are brittle, and can result in higher ON-resistance, when used as part of a switched circuit. These limitations have been partially addressed by the advent of actuators made from selectively doped single-crystal silicon [7]. The selective doping of these silicon devices can potentially reduce their ON-resistance while maintaining the larger temperature difference in the two actuating arms of the switch.

In comparison to (poly)silicon devices, metallic thermal micro-actuators have a larger thermal expansion coefficient and can thus undergo larger deformations for a given temperature difference. Alternatively, since the power required for keeping the switch closed is dependent on the heat dissipation to the surroundings, for a given stroke, the metal actuator will operate at a lower temperature resulting in a lower steady-state power consumption. Improvements in power consumption can also be achieved by modifying the nature of the underlying substrate. While most thermal actuators are fabricated on silicon substrates, it is possible to develop similar devices directly onto printed circuit boards, as is shown in this paper. The integration of the MEMS structures onto the printed circuit board has several advantages:

- Metal-ion contamination of semiconductor devices is avoided.
- The process is compatible with RF and microwave copper circuit fabrication.
- There is no need to modify the existing integrated circuit processes in order to incorporate the MEMS structures in them.
- Reduced power consumption.
- Simpler and inexpensive fabrication process.

* Corresponding author. Tel.: +1-520-621-4506; fax: +1-520-621-8191.
E-mail address: enikov@engr.arizona.edu (E.T. Enikov).

0924-4247/03/$ – see front matter © 2003 Elsevier Science B.V. All rights reserved.
doi:10.1016/S0924-4247(03)00065-7

High fabrication costs are one of the major roadblocks in the establishment of a new technology. Except for a few success stories, the high cost of the process modifications necessary to integrate Si-based MEMS structures into existing IC layouts prevents the widespread use of this technology. Fortunately, microwave circuits containing tunable filters, RF switches, and wave-guide elements have characteristic sizes on the order of 10–15 μm. Therefore, a fabrication process capable of generating such feature sizes would be an ideal candidate for building RF MEMS. This was our motivation in investigating the possibility of using an electroforming technique to generate functional micro-actuators directly onto a printed circuit board.

2. Thermal micro-actuators design and operation

2.1. Static deformation analysis

The geometry of a typical micro-actuator is shown in Fig. 1. There are two types of actuators: thermal bimorphs, in which two different thermal expansion coefficient materials are used, and homogeneous actuators, in which a temperature difference is set between the narrower "hot" and the wider "cold" arm. In both devices, a bending moment is created in the two beams, and the two-arm structure deflects towards the beam with smaller expansion. In this paper, we describe an actuator of the latter type. Using linear Euler–Bernoulli beam theory [9], the free-beam deflection, δ, of the actuator can be estimated as

$$\delta \approx \frac{(\alpha(T)\Delta T)(l_c)hw(w+g)(2l_f l_c + l_f^2)}{2(2l_f + l_c)I};$$
$$I = \frac{2}{3}h\left[\left(w+\frac{g}{2}\right)^3 - \left(\frac{g}{2}\right)^3\right], \quad (1)$$

where $\alpha(T)$ is the thermal expansion coefficient; $\Delta T = T^{\text{hot}} - T^{\text{cold}}$, where T^{hot} and T^{cold} are the temperatures of the "hot" and "cold" arms respectively; g is the gap between the hot arm and the flexure; and I the second-order moment of the double cross-section (denoted as flexure in Fig. 1). We have further assumed that the widths of the hot arm and the flexure are equal, $w = w_h = w_f$ (see Fig. 1), since this is a common case in practical applications. For the sake of simplicity, in the following we have approximated the temperature-dependent thermal expansion coefficient with its mean value $\alpha(T)\,\Delta T \approx \bar{\alpha}\,\Delta T = \int_0^{\Delta T}\alpha(T)\,\mathrm{d}T$.

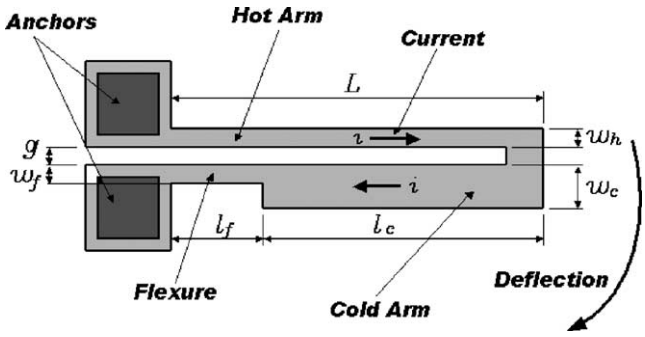

Fig. 1. Thermal micro-actuator.

bending occurs in the flexure section only. The linear analysis temperature limit can be obtained from the buckling condition

$$\bar{\alpha}\,\Delta T\,Ewt \le \frac{4\pi^2 E(tw^3/12)}{L^2} = F_{\text{crit}}^{\text{buck}} \quad \text{or} \quad \bar{\alpha}\,\Delta T \le \frac{\pi^2 w^2}{3L^2}. \quad (2)$$

Surprisingly, condition (2) is easy to violate. Using the data for our actuator ($w = 15\,\mu\text{m}$, $L = 600\,\mu\text{m}$, $\bar{\alpha} = 13.1 \times 10^{-6}$) results in $\Delta T \le 157\,^{\circ}\text{C}$, indicating that for higher temperature rises a non-linear buckling analysis should be performed in order to establish the exact beam displacement.

2.2. Transient analysis

Response time is an important characteristic of any actuator. Two transient phenomena determine the total response time of a thermal actuator: (1) transient heating and cooling and (2) mechanical acceleration/deceleration. The mechanical (inertial) time constant of the actuator is dependent upon the air damping, the stiffness, and the mass of the beam. According to the theory of flexural vibrations of thin beams [10,11], the lateral displacement, $v(x,t)$, of an elastic beam is described by

$$v(x,t) = \sum_{j=1}^{\infty}(a_j S(\lambda_j x) + b_j T(\lambda_j x) + c_j U(\lambda_j x) + d_j V(\lambda_j x))\sin(\omega_j t + \varphi_j), \quad (3)$$

where $S(x) = (\cosh x + \cos x)/2$, $T(x) = (\sinh x + \sin x)/2$, $U(x) = (\cosh x - \cos x)/2$, and $V(x) = (\sinh x - \sin x)/2$ are the Krulov eigenfunctions and j indicates the mode of vibration. Eq. (3) is applied separately for each section of the beam—flexure, cold arm, and hot arm (Fig. 1)—with the following boundary conditions:

$$\begin{aligned}
&v(0,t) = 0, \quad v'(0,t) = 0 && \text{at bonding pads}\\
&v(x,t), \quad v'(x,t), \quad v''(x,t) \quad \text{and} \quad v'''(x,t) && \text{continuous at flexture/cold-arm junction}\\
&v^{\text{hot arm}}(L,t) = v^{\text{cold arm}}(L - l_f, t), \quad v'^{\text{hot arm}}(L,t) = v'^{\text{cold arm}}(L - l_f, t) && \text{at the free end}
\end{aligned} \quad (4)$$

The analysis above assumes that the thermal load is below the buckling stability limit of the hot arm and that the

Seeking a non-zero solution for the unknown coefficients, a_i, b_i, c_i and d_i, for each section of the beam, Eq. (3)

was used to match the boundary conditions (4). The resulting system of eight equations produced a singular system matrix, which is the so-called a non-linear characteristic equation for the natural frequencies of vibration ω.

$$\det\begin{bmatrix} U(\lambda_f l_f) & V(\lambda_f l_f) & -1 & 0 & 0 & 0 & 0 & 0 \\ \lambda_f T(\lambda_f l_f) & \lambda_f U(\lambda_f l_f) & 0 & -\lambda_c & 0 & 0 & 0 & 0 \\ \lambda_f^2 S(\lambda_f l_f) & \lambda_f^2 T(\lambda_f l_f) & 0 & 0 & -\lambda_c^2 & 0 & 0 & 0 \\ \lambda_f^3 V(\lambda_f l_f) & \lambda_f^3 S(\lambda_f l_f) & 0 & 0 & 0 & -\lambda_c^3 & 0 & 0 \\ 0 & 0 & S(\lambda_c l_c) & T(\lambda_c l_c) & U(\lambda_c l_c) & V(\lambda_c l_c) & -U(\lambda_h L) & V(\lambda_h L) \\ 0 & 0 & \lambda_c V(\lambda_c l_c) & \lambda_c S(\lambda_c l_c) & \lambda_c T(\lambda_c l_c) & \lambda_c U(\lambda_c l_c) & -\lambda_h T(\lambda_h L) & -\lambda_h U(\lambda_h L) \\ 0 & 0 & \lambda_c^2 U(\lambda_c l_c) & \lambda_c^2 V(\lambda_c l_c) & \lambda_c^2 S(\lambda_c l_c) & \lambda_c^2 T(\lambda_c l_c) & -\lambda_h^2 S(\lambda_h L) & -\lambda_h^2 T(\lambda_h L) \\ 0 & 0 & \lambda_c^3 T(\lambda_c l_c) & \lambda_c^3 U(\lambda_c l_c) & \lambda_c^3 V(\lambda_c l_c) & \lambda_c^3 S(\lambda_c l_c) & -\lambda_h^3 V(\lambda_h L) & -\lambda_h^3 S(\lambda_h L) \end{bmatrix} = 0. \quad (5)$$

Eq. (5) is a scalar equation for the natural frequency ω, which is related to λ_f, λ_c, and λ_h through $\lambda_i^4 = \omega^2 \rho A_i / E I_i$, $i = f, c, h$ with A_i and I_i being the cross-sectional area and second-order moment, respectively. Eq. (5) was solved numerically in MATLAB, using the the geometry of the fabricated actuator ($L = 600\,\mu\text{m}$, $l_f = 200\,\mu\text{m}$, $l_c = 400\,\mu\text{m}$, $w_f = w_h = 15\,\mu\text{m}$, $w_c = 25\,\mu\text{m}$). For nickel, the resulting lowest natural frequency of the beam was $f = \omega/2\pi = 37.89\,\text{kHz}$. Modal analysis with ANSYS resulted in $f = 37.82\,\text{kHz}$, showing a 0.2% error between the two simulations. To estimate the response time, we use the rise-time of a second-order system, defined as the time required to go from 10 to 90% of the system's steady-state value. Assuming that the mechanical dynamics of the thermal beam is described reasonably well by a second-order model, the rise-time can be estimated as [12]

$$\tau_{\text{mech}} = \frac{1.8}{\omega} = \frac{1.8}{2\pi f}. \quad (6)$$

For nickel, (6) gives $\tau_{\text{mech}} \approx 7.5\,\mu\text{s}$.

The thermal transient behavior of the actuator can be approximately modeled as a one-dimensional beam (slab) in contact with an infinite-capacity thermal reservoir (the substrate or a large bonding pad). Neglecting the convective and radiative cooling,[1] the temperature distribution is [14]

$$T(x,t) = 2T_{\text{ON}} \sum_{n=1}^{\infty} \frac{e^{-\alpha\beta_n^2 t}}{L\beta_n} \sin(\beta_n x), \quad L\beta_n = \frac{(2n-1)\pi}{2}, \quad (7)$$

where $\alpha = k/\bar{C}_p\rho$ is the thermal diffusivity, T_{ON} the temperature of the arm during the "ON" period, ρ the mass density, and $\bar{C}_p$ the mean specific heat capacity. Simple averaging shows that the beam's mean temperature and cooling time constants are given by

$$\bar{T}(t) = \frac{8T_{\text{ON}}}{\pi^2} \sum_{n=1}^{\infty} \frac{e^{-\alpha\beta_n^2 t}}{(2n-1)^2} = \frac{8T_{\text{ON}}}{\pi^2} \times \left(\frac{e^{-(\alpha\pi^2 t)/(4L^2)}}{1} + \frac{e^{(-9\alpha\pi^2 t)/(4L^2)}}{9} + \cdots \right), \quad (8)$$

$$\tau_{\text{cooling}} = \frac{4L^2}{\alpha\pi^2}. \quad (9)$$

For nickel and copper, (9) results in $\tau_{\text{cooling}} = 9.5$ and 1.4 ms, respectively. This approximate analysis compares very favorably with the experimentally measured 10 ms cooling time constant for Ni on printed circuit board (PCB) substrate. The above analysis assumes that the substrate has high thermal conductivity, which is a good assumption for Si and somewhat less accurate for PCB substrates. However, the measured time constant is close to the predicted one, even though the thermal conductivity of the PCB substrate (0.5 W/mK) is 300 times lower than the corresponding value for Si (150 W/mK). The relative insensitivity of the time constant with respect to the conductivity of the substrate is the large area of the bonding pads ($1000\,\mu\text{m} \times 800\,\mu\text{m}$) compared to the cross-section of the hot arm ($15\,\mu\text{m} \times 16\,\mu\text{m}$).

A finite element (FE) transient analysis has also been performed using ANSYS. The FE model of the actuator used the three-dimensional tetrahedral coupled-field elements SOLID98, with five active degrees of freedom: temperature, displacements (u_x, u_y, u_z), and voltage potential. The displacement and temperature distribution results of these simulations are shown in Fig. 2. A maximum displacement of 12.1 μm was predicted using a 0.15 V driving voltage, which resulted in a mean temperature difference of approximately 125 °C. Table 1 lists the estimated mechanical rise-times for several materials. As evident from the table, the predicted thermal time constant is three orders of magnitude larger than the mechanical rise-time and thus

[1] Reported estimates indicate that convection is responsible for only 5–10% of the total heat flux [13].

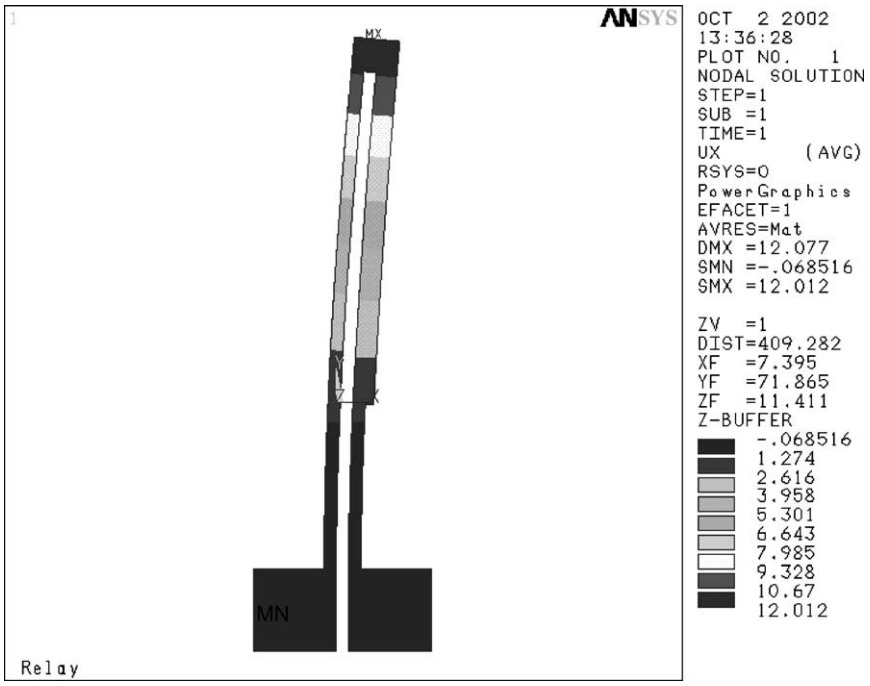

Fig. 2. Lateral displacement due to $\Delta T_{ON} = 125\,^{\circ}C$ (gray-scale colors indicate displacement).

Table 1
Estimated maximum displacements and time constants for $L = 600\,\mu m$, $w_h = w_f = 15\,\mu m$, and $w_c = 25\,\mu m$ actuator, made of several common materials (Fig. 1)

Material	Thermal expansion coefficient	Thermal diffusivity (m^2/s)	Free-beam deflection (μm) ($\Delta T = 125\,^{\circ}C$) (Eq. (1))	Mechanical rise-time (μs) (Eqs. (5) and (6))	Cooling time constant (ms) (Eq. (9))
Nickel	13.1×10^{-6}	1.55×10^{-5}	13.3	7.5	9.5
Copper	17.5×10^{-6}	1.03×10^{-4}	17.5	9.4	1.4
Single-crystal Si	2.33×10^{-6}	9.0×10^{-5}	3.61	3.9	1.6

determines the overall response time of the actuator. Since, in the majority of applications the instantaneous input power to the device can be sufficiently large to ensure short heating times, the critical factor remains the time required to cool the actuator. According to our experimental and theoretical predictions for the current geometry, this time constant is approximately 1–10 ms limiting the bandwidth of these devices to 100–1000 Hz.

3. Fabrication sequence

The fabrication of a thermal micro-actuator onto a PCB is shown in Fig. 3. We used microwave-grade PCBs (RO-3000 series, Rogers Corporation, Microwave Materials Division, Chandler, AZ) with approximately 15 μm of laminated copper. The microwave PCBs typically have smoother surfaces in order to reduce transmission losses. A single photolithography step was used to form a photoresist mold (AZ4903, Clariant Corporation, NJ) for the electroplating of Ni, which resulted in structures with aspect ratios in the range of 0.3–1, depending on the length of plating. In the case of

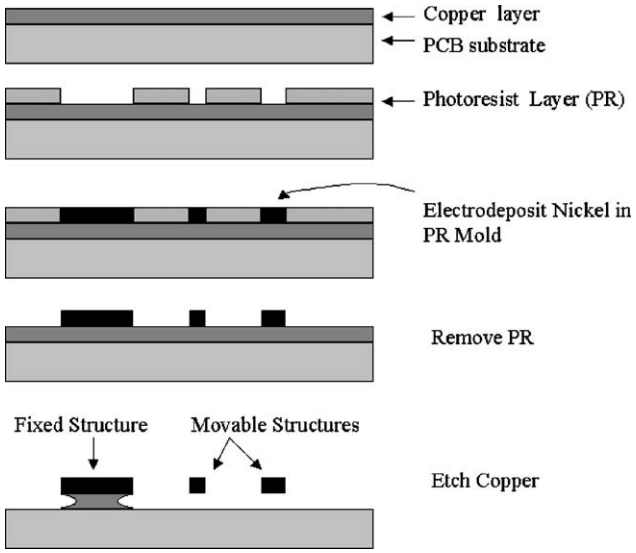

Fig. 3. Fabrication sequence.

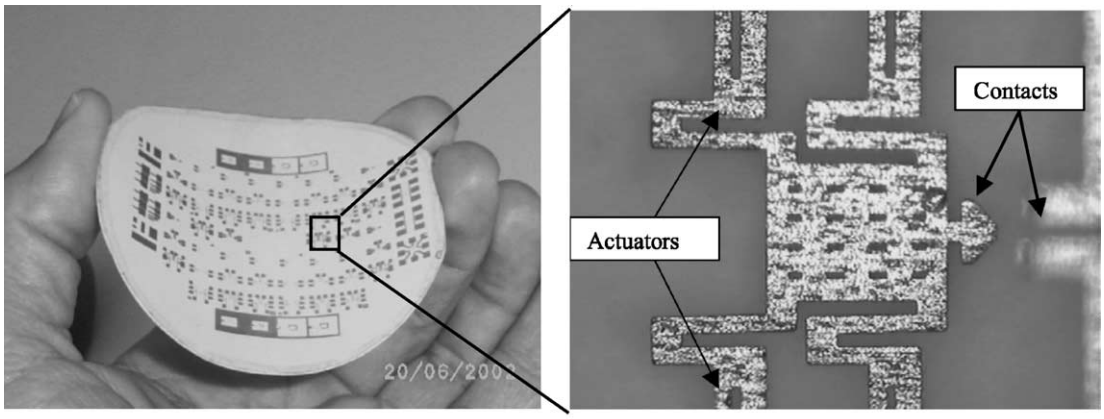

Fig. 4. Fabricated test devices: (a) flexible PCB substrate; (b) four-arm micro-actuator structure (SU8-based process).

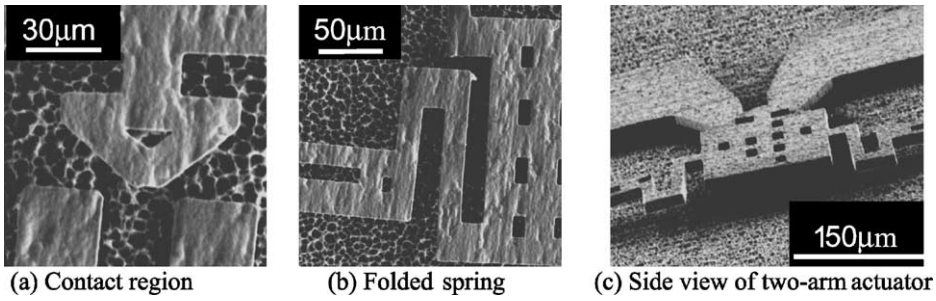

Fig. 5. SEM photomicrographs of fabricated actuators (SU8-based process).

photoresist, the slope of the side walls has not been investigated. A commercial nickel sulfamate plating bath, Microfab Ni100 (Enthone, RI), was used to deposit 16.5 μm of nickel, using a 290 mA (1.1 ASD) deposition current over a 65 min plating time. The actuator release was achieved via timed wet etching of the underlying copper in $(NH_4)_2S_2O_8$ solution [15]. During this step, the wider features are not completely undercut and are therefore fixed to the underlying substrate in order to anchor the device. In comparison with usual fabrication processes, the use of PCB substrates results in a rougher surface, due to the roughness of the underlying substrate. This limits the minimum feature size to 5–10 μm. The fabricated test devices are shown in Fig. 4. Fig. 4a shows the entire PCB wafer, and Fig. 4b shows an individual device. We have also completed the same process using SU8 photo-epoxy instead of photoresist. To aid the SU8 removal process we used a polymer sacrificial layer Omnicoat™ (Microchem, MA) prior to depositing the SU8 mold, as recommended by the manufacturer. This modification resulted in structures with higher aspect ratios and vertical sidewalls. Fig. 5a-c show SEM micrographs of the contact region of a micro switch, the folded spring, and the entire actuator produced with the SU8 process. As evident from Fig. 5c, which was taken after the actuators were energized, an undesirable out-of-plane displacement has been observed due to the lower buckling stiffness in this direction. Our simulations indicate that this undesirable effect can be reduced/eliminated by increasing the height of the structures to 25 μm.

Table 2
Measured two-arm actuator characteristics

Parameter	Value
Displacement (μm)	13
Arm length (total) (μm)	600
Operating current (A)	0.210 (per actuator)
Operating voltage (V)	0.21
Resistance (Ω)	1.0 (per actuator)

4. Performance measurements

The following performance parameters were measured: power consumption, displacement, and response time. As discussed earlier, the response time is determined to be the cooling transient, thus we have limited the measurements to thermal effects only. Power consumption was measured by recording the voltage drop and current through the device, and the stroke was measured optically using a calibrated vernier on the substrate. A summary of the measured data is provided in Table 2.

The cooling time was measured using a two-step technique. First, the actuator is energized at high current, which

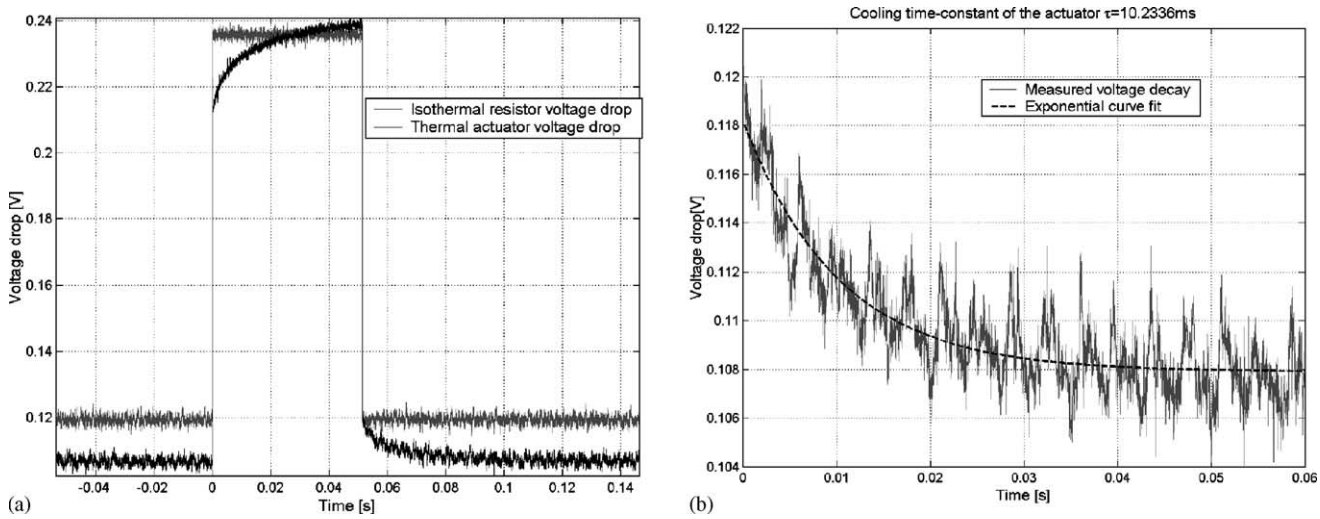

Fig. 6. Voltage drop: (a) across thermal actuator and reference resistor; (b) thermal constant extraction via non-linear curve fit.

is later reduced to a lower value. During the second step, the voltage drop across the actuator is measured at constant current. Due to the temperature dependence of the resistance of the metal, the cooling transient is captured in the voltage drop time history. There is no need to know the exact value of the temperature resistance coefficient α_T, since we are interested in the time required to cool the actuator. Assuming a linear resistance–temperature relationship, the total resistance is given by

$$R(\bar{T}) = R_0 + \alpha_T \bar{T}, \tag{10}$$

where R_0 is the room temperature resistance and α_T the temperature resistance coefficient. The voltage drop at constant current, I_0,then is

$$U(\bar{T}) - U_0 = I_0 \alpha_T \bar{T} \tag{11}$$

where $U_0 = R_0 I_0$ is the room temperature ($\bar{T} = 0$) voltage drop. A two–level current source (built in house) was used to supply 120 and 240 mA of current to the thermal actuators. Fig. 6a shows the voltage time history across a 1 Ω isothermal reference resistor (gray curve) and across the thermal actuator. Fig. 6b shows the cooling phase of Fig. 6a. The time constant of the cooling step was determined by fitting an exponential decay function of the form $V(t) = V_0 + V_a\, e^{-t/\tau}$ to the experimental data by minimizing the quadratic error. The resulting curve is also shown in Fig. 6b with time constant $\tau = 10.2$ ms. Comparison with the projected values in Table 1 shows agreement within 10%.

The actuator displacement was measured optically using a calibrated CCD camera. The measured displacements were in good agreement with the FE predictions. The differences between 13 μm (measured) and 12.01 μm (ANSYS) and 13.3 μm (from Eq. (1)) are most likely due to the relatively poor prediction of the temperature distribution, as well as the approximate nature of Eq. (1). The importance of a precise knowledge of the temperature distribution was observed from a comparison between identical actuators fabricated on silicon and PCB substrates. A noticeable difference in the temperature distribution (observed by color change in the nickel) was observed in the case of highly thermally conductive silicon substrates, which showed significantly enhanced heat flux across the thin layer of air between the actuator and the substrate. In the case of large-surface-area devices such as the one shown in Fig. 4b, the heat flux toward the substrate should be taken into account. Such observation was also shown by Lott et al. [16], and indicates that the heat flux towards the substrate in our case might exceed the estimates reported by other groups [13].

5. Conclusions

A process for fabricating MEMS micro-actuators directly onto printed circuit boards has been described. In this work the device yield could not be measured due to the low number of identical dies on the substrate. The device yield is controlled by the successful release of the SU8 layer. In related application [17] using the same process on a Si substrate, the authors achieved a device yield of approximately 85%. The minimum feature size of these actuators is in the range of 10–15 μm, which is acceptable for RF applications. The achieved aspect ratio is approximately one when the standard photoresist was replaced by SU8. For the fabricated 16.5 μm-thick devices, some out-of-plane displacement was observed, which is attributed to the low out-of-plane stiffness of the structures. While this effect prevents sticking of the structures and facilitates their release, it is detrimental to the micro-relay application and can result in poor electrical contacts. For the given geometry an increase of the height to 20–25 μm by using a thicker SU8 layer should reduce this effect [17].

Analytical approximations of the mechanical and thermal response times showed that thermal cooling limits the bandwidth of the thermal actuators to below 1000 Hz.

Commercial application of the fabricated PCB-based MEMS will require development of new packaging schemes. The demonstrated process removed the underlying copper from the entire substrate, which is unacceptable for a real PCB. A straightforward masking step should be included in order to protect the rest of the PCB circuit during the release step. This will allow a straightforward integration of the MEMS-based switches with drivers and other discrete electronic components.

References

[1] E.R. Brown, RF-MEMS switches for reconfigurable integrated circuits, IEEE Trans. Microwave Theory Techniq. 46 (11) (1998) 1868.
[2] K.E. Peterson, Micromachined membrane switches on silicon, IBM J. Res. Develop. 23 (1979) 376–385.
[3] L.E. Larson, R.H. Hacket, M.S. Melendes, R.F. Lohr, Micromachined microwave actuator (MI-MAC) technology—a new tuning approach for microwave integrated circuits, in: Proceedings of the IEEE Microwave Millimeter-Wave Monolithic Circuits Symposium, Boston, MA, June 1991, pp. 27–30.
[4] A. Paultre, Microrelay brings MEMS technology to commercial market, Electronic Products, February 1999, p. 28.
[5] H. Guckel, et al., Thermo-magnetic metal flexure actuators, in: Proceedings of the Fifth IEEE Solid State Sensors and Actuator Workshop, Hilton Head Island, SC, USA, 22–25 June 1992, pp. 73–75.
[6] J.M. Noworolski, E.H. Klaassen, J.R. Logan, K. Peterson, N.I. Maluf, Process for in-plane and out-of-pale single-crystal-silicon thermal micrioactuators, Sens. Actuators A 55 (1996) 65–69.
[7] Dhuler et al., In plane MEMS thermal actuator and associated fabrication method, US Patent 6,211,598 (2001).
[8] X.Q. Sun, X. Gu, X. Carr, Lateral in-plane displacement microactuators with combined thermal and electrostatic drive, in: Proceedings of the Solid State Sensor and Actuator Workshop, Hilton Head, South Carolina, 2–6 June 1996.
[9] J.H. Faupel, F.E. Fisher, Engineering Design: A Synthesis of Stress Analysis and Materials Engineering, second ed., Wiley, New York, 1981.
[10] E.T. Enikov, Structures and materials, in: R. Bishop (Ed.), Handbook of Mechatronics, CRC Press, Boca Raton, FL, 2001.
[11] S. Timoshenko, S. Woinowsky-Krieger, Theory of Plates and Shells, McGraw-Hill, New York, 1959.
[12] G.E. Franklin, J.D. Powell, A. Emami-Naemi, Feedback Control of Dynamical Systems, Addison-Wesley, Reading, MA, 1991.
[13] Q.A. Huang, N.K. Shek Lee, Analysis and design of polysilicon thermal flexure actuator, J. Micromech. Microeng. 9 (1999) 64–70.
[14] O. Necati, Heat Conduction, Wiley, New York, 1980.
[15] J.L. Vossen, W. Kern, Thin Film Processes, Academic Press, New York, 1978.
[16] C. Lott, T. McLain, J. Harb, L. Howell, Modelling the Thermal behavior of a surface-micromachined linear-displacement thermomechanical actuator, Sens. Actuators: A Phys. 101 (1–2) (2002) 239–250.
[17] E.T. Enikov, K.V. Lazarov, G.R. Gonzales, Microelectrical mechanical systems actuator array for tactile communication, IC-CHP 2002 Lecture Notes in Computer Science, vol. 2398, 2002, pp. 551–558.

Biographies

Dr. Enikov received his MSc degree from Technical University of Budapest in 1993 and PhD degree from University of Illinois at Chicago in1998. His research is focused on the design and fabrication of micro-electromechanical systems (MEMS) as well as developing theoretical models of multi-functional materials used in MEMS. As a postdoctoral associate at University of Minnesota, Dr. Enikov has worked on several projects in the area of micro-assembly, capacitive force sensing. Currently Dr. Enikov is an assistant professor at the Aerospace and Mechanical Engineering Department at the University of Arizona. His research efforts are in characterization of nano-scale phenomena in smart materials as applied to MEMS.

Kalin Lazarov received his MSc degree in physics from Sofia University in 2000. Currently, Mr. Lazarov is a research assistant at the Aerospace and Mechanical Engineering Department at the University of Arizona seeking a PhD degree in mechanical engineering. Mr. Lazarov's research is focused on developing more energy efficient micro-actuators based on polymer/metal composites.